Video Article

Analysis of Minerals Produced by hFOB 1.19 and Saos-2 Cells Using Transmission Electron Microscopy with Energy Dispersive X-ray Microanalysis

Lukasz Bozycki[1], Magdalena Komiazyk[1], Saida Mebarek[2,3,4,5,6], Rene Buchet[2,3,4,5,6], Slawomir Pikula[1], Agnieszka Strzelecka-Kiliszek[1]

[1]Laboratory of Lipid Biochemistry, Nencki Institute of Experimental Biology, Polish Academy of Sciences

[2]Université de Lyon

[3]Université Lyon 1

[4]L'insitut National des Sciences Appliquées (INSA) de Lyon

[5]Ecole Supérieure de Chimie Physique Electronique (CPE) Lyon

[6]Centre National de la Recherche Scientifique (CNRS), Unité Mixte de Recherche (UMR), L'institut de Chimie et Biochimie Moléculaires et Supramoléculaires (ICBMS)

Correspondence to: Agnieszka Strzelecka-Kiliszek at a.strzelecka-kiliszek@nencki.gov.pl

URL: https://www.jove.com/video/57423
DOI: doi:10.3791/57423

Keywords: Retraction, Issue 136, minerals, vesicles, osteoblasts, osteosarcoma, UV light, TEM-EDX

Date Published: 6/24/2018

Citation: Bozycki, L., Komiazyk, M., Mebarek, S., Buchet, R., Pikula, S., Strzelecka-Kiliszek, A. Analysis of Minerals Produced by hFOB 1.19 and Saos-2 Cells Using Transmission Electron Microscopy with Energy Dispersive X-ray Microanalysis. *J. Vis. Exp.* (136), e57423, doi:10.3791/57423 (2018).

Abstract

This video presents the use of transmission electron microscopy with energy dispersive X-ray microanalysis (TEM-EDX) to compare the state of minerals in vesicles released by two human bone cell lines: hFOB 1.19 and Saos-2. These cell lines, after treatment with ascorbic acid (AA) and β-glycerophosphate (β-GP), undergo complete osteogenic transdifferentiation from proliferation to mineralization and produce matrix vesicles (MVs) that trigger apatite nucleation in the extracellular matrix (ECM).

Based on Alizarin Red-S (AR-S) staining and analysis of the composition of minerals in cell lysates using ultraviolet (UV) light or in vesicles using TEM imaging followed by EDX quantitation and ion mapping, we can infer that osteosarcoma Saos-2 and osteoblastic hFOB 1.19 cells reveal distinct mineralization profiles. Saos-2 cells mineralize more efficiently than hFOB 1.19 cells and produce larger mineral deposits that are not visible under UV light but are similar to hydroxyapatite (HA) in that they have more Ca and F substitutions.

The results obtained using these techniques allow us to conclude that the process of mineralization differs depending on the cell type. We propose that, at the cellular level, the origin and properties of vesicles predetermine the type of minerals.

Video Link

The video component of this article can be found at https://www.jove.com/video/57423/

Introduction

Bone is a type of connective tissue composed of two parts: organic (cells and collagen fibers) and mineral (calcium and phosphate compounds). The main mineral components in bones are apatites[1]. Different types of mineralization-competent cells in bone (osteoblasts), in teeth (odontoblasts) and in cartilage (chondrocytes) regulate the initial steps of mineralization by producing proteins of the extracellular matrix (ECM) and releasing matrix vesicles (MVs) (**Figure 1**). MVs are 100-300 nm diameter vesicles that accumulate calcium and phosphate facilitating apatite nucleation and subsequently bind to collagen[2,3]. Then, MVs disintegrate to release apatites to the extracellular medium. The apatites continue to grow in contact with collagen fibers and form the bone matrix. The mineralization is sustained by the constant supply of P_i and Ca^{2+} in the extracellular medium. Some recently published data support our model[4,5]. Soft tissues do not mineralize under physiological conditions. However, ectopic calcification may occur under pathological conditions such as vascular calcification[3]. Vascular cells that acquire the osteoblast phenotype can produce MVs that induce nucleation of apatites and initiate mineralization in the medial and intimal layers of the wall of blood vessels. Since ectopic calcification resemble normal endochondral mineralization[3], understanding the molecular mechanisms of mineralization of osseous cells and chondrocytes should provide some clues on ectopic calcification of soft tissues that are formed.

The development of skeletal tissues is regulated by various enzymes, growth factors, and promoters or inhibitors of mineralization. The antagonistic action of tissue-nonspecific alkaline phosphatase (TNAP) (**Figure 1**) and ectonucleotide pyrophosphatase/phosphodiesterase I (NPP1), together with ankyrin (ANK), controls inorganic pyrophosphate (PP_i) concentration[6]. PP_i, a potent inhibitor of HA formation, is hydrolyzed by TNAP; NPP1 hydrolyzes nucleotide triphosphates to form PP_i while ANK exports PP_i from the cell to the ECM. The Pi/PPi ratio may regulate apatite formation[7,8] with possible pathological consequences[9].

The MV membrane is enriched in ion transport proteins that facilitate the initial precipitation of calcium and phosphate inside the MVs during the nucleation process (**Figure 1**). The phosphate transporter 1 (PiT) helps to incorporate P_i generated in the perivesicular space into the MVs[10,11]. Annexins may be involved in the binding and transport of Ca^{2+} and in the biophysical process that initiates mineralization in the MV lumen[12,13]. We favor the hypothesis, suggested earlier, for mineralization within intracytoplasmic vesicles of internal nucleation of apatite inside the MV before its propagation in the ECM[14,15]. *In vitro* modeling confirmed the induction of Ca^{2+}/P_i complexes formation in proteoliposomes made from PS and AnxA5[16]. This may indicate that accumulation of Ca^{2+}, P_i, AnxA5 and PS complexes in lipid rafts of microvilli-like membranesrepresent the nucleation core (NC) of apatite within M*Vs.* Annexins and TNAP also possess collagen-binding capacities that may be helpful in placing MVs along collagen fibers and, in stimulating the propagation of mineralization in the ECM. Fetuin A and osteopontin (OPN)[17], are known as inhibitors of apatite formation that may slow down the propagation of mineralization on the collagenous scaffold. Nucleation and propagation are distinct events, the former preceding the latter, and both may be relevant for the process of pathological mineralization.

To discover how the chemistry of calcium phosphate complexes may change physiological mineralization and ectopic calcification, it is necessary to identify the minerals produced by cells. Apatites are a group of calcium and phosphate containing minerals with the general crystal unit cell formula $Ca_{10}(PO_4)_6X_2$, where X = Cl, F, OH. They are classified as follows[18]: fluorapatite (FA) $Ca_{10}(PO_4)_6F_2$, chlorapatite (CA) $Ca_{10}(PO_4)_6Cl_2$ and hydroxyapatite (HA) $Ca_{10}(PO_4)_6(OH)_2$.

The choice of osteoblast cell lines to induce mineral formation is crucial, since each cell line exhibits a distinct profile of mineralization. In this report, we compared the nucleation of minerals by two selected human cell models of mineralization: osteoblastic hFOB 1.19 cells and osteosarcoma Saos-2 cells. Osteosarcoma-derived cells are commonly used as osteoblastic models and Saos-2 cells have preserved the most mature osteoblastic character[19] while undifferentiated human fetal hFOB cells are widely used as a model for normal osteoblastic differentiation[20]. Their mineralization profiles were analyzed by different methods: Alizarin Red-S (AR-S) staining, ultraviolet (UV) light visualization, transmission electron microscopy (TEM) imaging, energy dispersive X-ray microanalysis (EDX) quantitation, and ion mapping. The advantage of TEM-EDX over alternative techniques used in previous studies is that it gives quantitative and qualitative results of ion replacement in apatite crystals[4,5,21]. The overall goal of using TEM-EDX was to find a simple method for imaging and quantification of the distribution of Ca, F and Cl ions in various minerals from different types of cells during distinct stages of the mineralization process. This method has been successfully used, for example, for monitoring the interaction of zinc nanoparticles with coexisting chemicals and their combined effects on aquatic organisms[22]. In another study, a copper photocatalyst on titanium materials in aqueous solution was extensively characterized by means of inductively coupled plasma optical emission spectrometry (ICP-OES), N2 physisorption (BET), XRD, UV-vis DRS, FT-IR, Raman spectroscopy, TEM-EDX, and photoelectrochemical measurements[23]. Our aim was to compare the origin and properties of vesicles and minerals in two cell lines to understand the mechanism that controls mineralization during osseous differentiation.

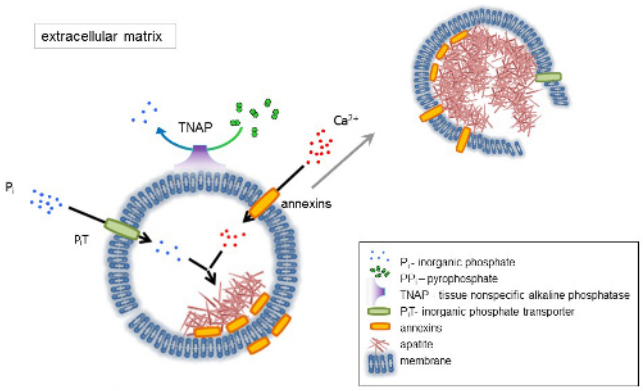

Figure 1. Scheme of the initial steps of mineralization in osseous cells involving the synthesis of extracellular matrix (ECM) proteins and release of matrix vesicles (MVs) from the membrane. MVs accumulate calcium through the action of calcium binding proteins, annexins and phosphate, through the action of an inorganic phosphate transporter (PiT) followed by the activity of tissue non-specific alkaline phosphatase (TNAP), which dephosphorylates PP_i to P_i, thereby facilitating apatite nucleation. Then, MVs disintegrate and release apatites to the extracellular medium. The mineralization is sustained by the constant supply of P_i and Ca^{2+} in the extracellular medium[4,5]. Please click here to view a larger version of this figure.

Protocol

1. Cell Culture and Treatment

1. Put all the necessary materials under the laminar flow hood and sterilize them under UV light. The culture media are: a 1:1 mixture of Ham's F12 and DMEM media with 2.5 mM L-glutamine supplemented with 100 U/mL penicillin, 100 U/mL streptomycin, 0.3 mg/mL G418 and 10% Fetal Bovine Serum (FBS) (v/v) for human fetus hFOB 1.19 SV40 large T antigen transfected osteoblasts, and McCoy's 5A medium with 1.5 mM L-glutamine supplemented with 100 U/mL penicillin, 100 U/mL streptomycin and 15% FBS (v/v) for human osteosarcoma Saos-2 cells.
2. Culture hFOB 1.19 cells at 34 °C in an atmosphere of 5% CO_2 and Saos-2 cells at 37 °C in an atmosphere of 5% CO_2. Transfer cell cultures, either hFOB 1.19 or Saos-2 cells, from the incubator to the laminar flow hood and change the medium to 10 mL of fresh culture medium with FBS.
3. Incubate cells without stimulators (resting cells) or stimulate them with 50 µg/mL Ascorbic Acid (AA) followed by 7.5 mM β-Glycerophosphate (β-GP), prepared earlier in ultrapure water and filtered through 0.22 µm syringe filters. Add the stimulators from plastic microcentrifuge tubes onto the surface of the culture medium. Gently stir the culture dish and incubate for 7 days.

2. Detection of Calcium Minerals

1. Wash the cell cultures with Phosphate Buffer Saline (PBS: 125 mM NaCl, 5 mM KCl, 10 mM Na_2HPO_4, 1 mM KH_2PO_4, pH 7.0).
2. Add 5 mL of 2% (g:100 mL) AR-S in PBS, pH 5.0 and incubate the plates for 30 min to stain the minerals.
3. Wash 3 times with PBS. Carefully add PBS to the dish wall, try not to destroy the minerals.
4. Observe calcium minerals under an inverted light microscope and take images.

3. Visualization of Probes under UV Light

1. For cell lysates, treat cell cultures, either resting or stimulated for 7 days, according to the collagenase digestion protocol[24].
2. Collect the medium from cell cultures and wash the cells with PBS.
3. Digest the cells with 3 mL of 500 U/mL collagenase in a solution of 0.25 M sucrose, 0.12 M NaCl, 0.01 M KCl, and 0.02 M Tris-HCl buffer, pH 7.45, at 37 °C for 3 h.
4. Mechanically scrape the cells, transfer them to plastic microcentrifuge tubes, and pass them 10 times through a 1 mL 40 U syringe with 0.5 × 16 needle.
5. Centrifuge the samples at 500 × g for 5 min.
6. Discard the supernatant and suspend the cell pellet in 500 µL of Synthetic Cartilage Lymph (SCL, 100 mM NaCl, 12.7 mM KCl, 0.57 mM $MgCl_2$, 1.83 mM $NaHCO_3$, 0.57 mM NaH_2PO_4, 5.5 mM D-glucose, 63 mM sucrose, 16.5 mM Hepes, pH 7.4).
7. Transfer the hydroxyapatite (HA), fluorapatite (FA) and chlorapatite (CA) powders from the bottles on the UV transilluminator with a spatula and use as controls.
8. Transfer the cell lysates from the plastic tubes with plastic tips and place carefully on the UV transilluminator.
9. Take images under visible and UV light.

4. Preparation of Probes for TEM-EDX

1. Preparation of minerals for negative staining
    1. Suspend 2.5 mg of synthetically produced HA, CA and FA minerals[25] in 500 µL of deionized water and incubate at 37 °C in an atmosphere of 5% CO_2 for 1 h.
    2. Take Formvar/Carbon 300 Mesh Ni grids from the box with antistatic forceps, place on a porcelain multi-well plate and drop 10 µL of HA, CA and FA suspensions on the grids.
    3. Dry the samples for 30 min at room temperature.

2. Preparation of resting and stimulated cells for embedding [26]
    1. Collect medium from the cell cultures and wash the cells with Physiological Desensitization (PD) medium (125 mM NaCl, 5 mM KCL, 10 mM $NaHCO_3$, 1 mM KH_2PO_4, 10 mM glucose, 20 mM HEPES, pH 7.4).
    2. Fix the cells with 5 mL of a mixture of 3% (g:100 mL) paraformaldehyde/1% (g:100 mL) glutaraldehyde in 100 mM sodium phosphate buffer, pH 7.2, for 1 h at room temperature under the fume hood.
    3. Wash the cells with 5 mL of 100 mM sodium phosphate buffer and gently remove the buffer after washing.
    4. In the dark room, postfix the samples with 2 mL of 1% (g:100 mL) osmium tetroxide in 100 mM sodium phosphate buffer, pH 7.2, for 20 min at room temperature under the fume hood.
    5. Remove osmium tetroxide and utilize it.
    6. Wash the cells with 5 mL of 100 mM sodium phosphate buffer.
    7. Then, dehydrate the samples in 5 mL aliquots of a graded ethanol solution series at room temperature: 25% (by vol.) for 5 min, 50% (by vol.) for 10 min, 75% (by vol.) for 15 min, 90% (by vol.) for 20 min. Finally use absolute ethanol twice and incubate for 30 min and 12 h.
    8. Mechanically scrape the cells from the plastic Petri culture dishes, collect into plastic microcentrifuge tubes and centrifuge the samples at 130 x g for 1 min.
    9. Remove the supernatants and suspend the cells in 1 mL of a mixture of the LR White resin and absolute ethanol at a volume ratio of 1:2.
    10. Mix well the content of the glass tubes before use and incubate for 30 min at room temperature.
    11. Centrifuge the samples at 130 x g for 1 min.
    12. Remove the supernatants and repeat the previous step using 1 mL of a 1:1 mixture of LR White resin and absolute ethanol.
    13. Mix well and incubate for 30 min at room temperature.
    14. Centrifuge the samples at 130 x g for 1 min.
    15. Remove the supernatants.
    16. Finally, add 1 mL of pure LR White resin to the samples twice and incubate for 1 h at room temperature in plastic tubes.
    17. Place 500 µL of each sample into gelatin capsules.
        NOTE: The samples are labeled using a small sheet of paper and a pencil so that the resin does not destroy the labels.
    18. Close the gelatin capsules, put them into plastic microcentrifuge tubes and centrifuge at 130 x g for 1 min in a swing-out rotor.
    19. Remove the capsules from the plastic tubes using a vacuum pump.
    20. Move the samples to the oven and polymerize at 56 °C for 48 h.
    21. Prepare the blocks by mounting them into the holder and trimming them to the pyramid.
    22. Put the holder into the ultramicrotome, attach the diamond Ultra 45° knife and fill it with deionized water; remember to clean the blade from incidental air bubbles.
    23. Then cut sections (700 Å) using the diamond knife onto the deionized water bath.
    24. Set the scraps using bovine eyelash and place them on the shiny side of the Formvar/Carbon 300 mesh Ni grid and dry them.
    25. Prepare 2.5% (by vol.) uranyl acetate in absolute ethanol in the dark under a fume hood. Keep the uranyl acetate in a lead container and remember not to pick up the sediment.

26. In the dark room, counterstain the grids of synthetic apatites and cell samples with 2.5% (by vol.) uranyl acetate in ethanol for 20 min at room temperature under the fume hood.
27. Wash the grids in 50% ethanol (by vol.), then in deionized water and dry at room temperature for 24 h. Finally, put the grids into the box.

5. TEM-EDX Analysis

1. TEM imaging by a transmission electron microscope (TEM) equipped with full range Energy Dispersive X-ray microanalysis (EDX) System and 11 Megapixel camera
    1. Prepare a beryllium holder for the observation of minerals and cells. Use antistatic tools.
    2. Remove the pair of screws and lift the beryllium plate and beryllium washer away from the rest of the retainer.
    3. Mount the grid, shiny side up, on the holder.
    4. Carefully place the beryllium washer and beryllium plate and screw the fastening screws tightly.
    5. Put the holder into the vacuum chamber and turn on the vacuum pump.
    6. Once a vacuum is achieved, gently insert the holder into the imaging chamber and turn on the beam.
    7. On the fluorescent monitor, set the aperture parameters of the microscope. Perform image astigmatism correction; set the zoom, focus, and frame; and take TEM images at a magnification of 50,000X.

2. STEM imaging and X-ray microanalysis for spectral and compositional analysis
    1. Insert the energy dispersive X-ray (EDX) detector into the scanning transmission electron Microscopy (STEM) imaging chamber.
    2. Adjust the sharpness of the image in the focus mode.
    3. Take STEM images at a magnification of 15,000X.
    4. Select a point in the sample for X-ray microanalysis and collect spectra.
    5. Obtain data by summing all atomic weights for all elements of the Periodic Table in the sample (as 100%) and signifying the content of selected elements: Ca, F, Cl, and P (as atomic%). Then, calculate the ratios of Ca, F or Cl to P for each sample.

3. Ion mapping
    1. Select elements such as calcium, fluorine, chlorine and phosphorus to make ion mapping and perform EDX maps of the selected elements in the samples.
    2. Obtain data by indicating the localization of analyzed elements: Ca, F, Cl, and P (as atomic %) and calculate the co-localization (in %) of Ca, F or Cl with P for each sample.

Representative Results

TEM-EDX allows for the *in vitro* imaging of matrix vesicles (MVs) released by mineralizing cells and of minerals produced by M*Vs*. The results obtained using this technique demonstrate that the process of mineralization may proceed differently in various types of cells. The two cell lines received the same osteoblastic transdifferentiation treatment, yet stimulated Saos-2 cells mineralized more efficiently than hFOB 1.19 osteoblasts, as evidenced by AR-S staining (**Figure 2**). This might be due to the more mature osteoblast phenotype of Saos-2 cells[19] in comparison to hFOB 1.19 cells[20]. The visualization of samples using a UV transilluminator made it clear that only fluorapatites can be observed under UV light (**Figure 3**). TEM images indicated that stimulated Saos-2 cells produce more vesicles containing minerals compared to stimulated hFOB cells or with resting Saos-2 cells (**Figure 4**, left and middle panels). Synthetic apatites have different forms of minerals (**Figure 4**, right panel). TEM images showed the presence of vesicles in hFOB 1.19 and Saos-2 cells under resting and stimulated conditions (**Figure 5**, left panel). On EDX ion maps, red points indicate calcium, green points show phosphorus and blue points point to the fluorine distributions (**Figure 5**, middle panel). Under stimulated conditions, there is a strong overlap between calcium and phosphorus distributions in vesicles produced by Saos-2 cells and between fluorine and phosphorus in vesicles produced by hFOB 1.19 cells (**Figure 5**, right panel).

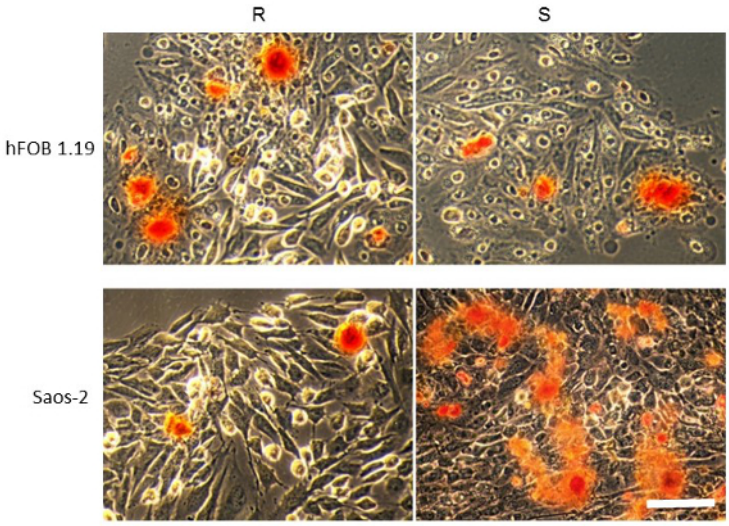

Figure 2. AR-S staining of minerals (red) produced by hFOB 1.19 (upper panel) and Saos-2 (bottom panel) cells either resting (R) or after 7 days of stimulation with AA and β-GP (S). Bar: 25 µm. A typical result with *n* = 3 is presented. Please click here to view a larger version of this figure.

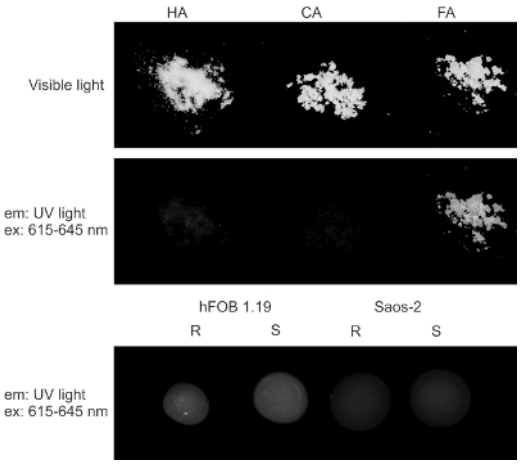

Figure 3. Visible (upper panel) and UV (middle panel) light visualization of synthetic HA, CA and FA minerals and of minerals produced by hFOB 1.19 (bottom left panel) and Saos-2 (bottom right panel) cells either resting (R) or after 7 days of stimulation with AA and β-GP (S). Please click here to view a larger version of this figure.

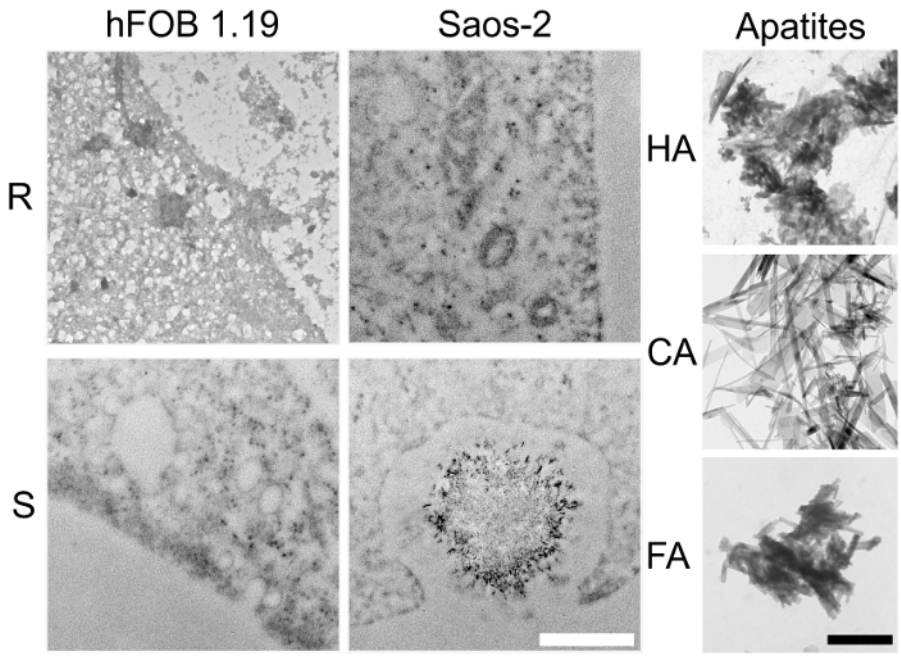

Figure 4. TEM images of vesicles and minerals produced by hFOB 1.19 (left panel) and Saos-2 (middle panel) cells either resting (R) or after 7 days of stimulation with AA and β-GP (S). Synthetic HA, CA and FA minerals are shown as controls (right panel). Bar: white 500 nm, black 250 nm. Please click here to view a larger version of this figure.

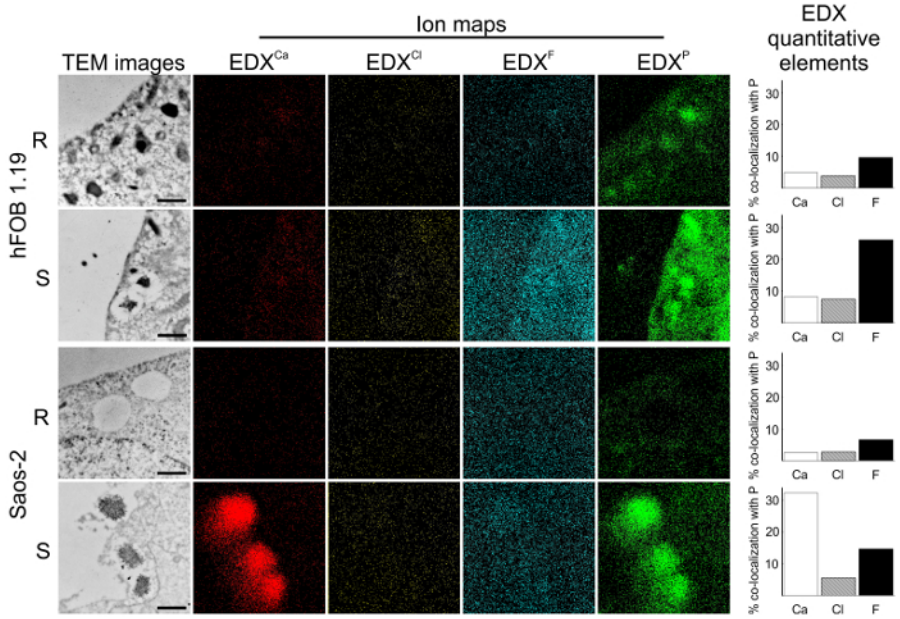

Figure 5. TEM images (left panel) of hFOB 1.19 and Saos-2 cells either resting (R) or after 7 days of stimulation with AA and β-GP (S). Ion maps for Ca (red), Cl (yellow), F (blue) and P (green) from EDX (middle panel). Co-localization of elements (right panel): calcium to phosphorus (Ca), fluorine to phosphorus (F), or chlorine to phosphorus (Cl) was quantified based on the EDX maps. Bar: 500 nm. Three independent experiments for both cell lines were performed. Ten pictures from each variant (resting and stimulated) were taken, then from 2 to 6 of them were selected for further calculation of element co-localization. One typical result is presented. Please click here to view a larger version of this figure.

Discussion

In the current paper, we described the protocols for AR-S staining, UV light identification of fluorapatite and TEM-EDX *in vitro* imaging of MVs released by mineralizing cells and of minerals produced by MVs. It is possible to address all methods mentioned above by following some common troubleshooting steps. In order to obtain optimal results, several critical steps should be performed carefully. First, it is better to add AA (which is acidic) followed by β-GP (which is alkaline) to preserve the pH 7.4 of the culture medium. Second, after AR-S staining, the stained calcium deposits are very fragile and the cells should be washed with great care to prevent destruction of the crystals upon adding PBS. Third, always keep the uranyl acetate in a lead container and do not pick up the sediment because only the diluted fraction should be used for fixation.

Fourth, remember that AA and uranyl acetate are light sensitive and should be handled in the dark room. Fifth, the mixture of LR White with absolute ethanol should be mixed well before being added to the samples. Sixth, the samples in gelatin capsules ought to be labeled using a small sheet of paper and a pencil so that the resin does not destroy the labels. Seventh, the blade of the diamond knife should be carefully cleaned from any air bubbles. Eighth, samples should be placed cautiously on the shiny side of the grid where the Formvar/Carbon film is situated. Ninth, position correctly the point at which X-ray microanalysis and ion mapping is performed at the TEM image to limit possible problems with apatite recognition.

Although the presented protocol proved to be most favorable in our experimental design, it is possible to modify it to fit different goals. As with any other technique, this one also has its limitations. Additional techniques, such as FTIR, should be applied to confirm or verify the existence of the obtained ratio of the examined elements[8,12,26]. The TEM-EDX method presented here is a significant improvement with respect to the existing method, which is a combination of micro-Raman-based mapping and chemometric methods and is similar to imaging of silver nanoparticles (AgNPs) distribution to various surfaces of mineral and the mechanism of their molecular interactions[21]. Raman-based imaging has been tested on two mineral models (macro- and micro-sized). Raman maps made of n = 600-900 spectra for each sample/control were analyzed by Vespucci software and the results were confirmed via other methods such as ICP-OES, AFM, and SEM-EDX. Our TEM-EDX maps comprising n = 30 frames and n = 6 spectra for each sample/control were also analyzed by the Microanalysis Suite software, and the results were confirmed via other methods such as FTIR, FM, TEM, SPM and 3D topographic AFM[4,5]. The proposed TEM-EDX microanalysis, like Raman-based imaging, requires only minimum sample preparation, is super-sensitive, non-invasive, and cost-effective, and may be extended to other systems relevant to the human environment.

The presented technique might be used in a wide field of research in the future. It may be modified for the investigation of different natural and synthetic apatites. It may also be adjusted to fit the protocols of experiments with biological and chemical probes. Furthermore, all elements from the Periodic Table can be analyzed in order to visualize not only the morphology of minerals but also changes in their ion composition and substitutions. Ion exchange in apatites is a known procedure for biomedical application[27]. One possible physiological factor that controls the Ca, F and Cl ions or Sr, Mg, Mn and Zn metal ion replacement in the HA during mineral formation, which is a turning point between physiological and pathological mineralization, may be the P_i/PP_i ratio[7]. If applied properly, this technique allows for performing the mapping of multiple elements of the same cellular, vesicular or mineral region several times in a row.

In recent years, much progress was made concerning the mechanisms of bone mineralization[28,29,30,31,32,33]. We realized that different cell lines may have distinct profiles of vesicles and mineral formation. In this regard, we selected two human cell lines: osteoblastic hFOB 1.19 and osteosarcoma Saos-2, which undergo complete osteogenic transdifferentiation from proliferation to mineralization and produce MVs that trigger apatite nucleation in ECM [34,35].

AR-S staining of calcium deposits revealed that stimulated Saos-2 cells mineralized differently than hFOB 1.19 osteoblasts. This was correlated with the production of minerals by Saos-2 cells that were undetectable under UV light in contrast to those produced by hFOB 1.19 cells. Our TEM-EDX data revealed that the minerals produced in vesicles of Saos-2 cells were similar to synthetic HA due to the overlap in calcium and phosphorus distributions. In contrast, the overlap in fluorine and phosphorus distributions in vesicles from hFOB 1.19 cells indicated the formation of other types of minerals in addition to apatites.

In conclusion, our findings indicate that the vesicles are key determinants of mineral nucleation, especially at the cellular level[5,25]. Moreover our data are in agreement with an earlier theory that MVs can be regarded as a specialized form of microvesicles that are able to start mineralization inside as well as outside the cell[4]. The comparison of vesicles released from Saos-2 cells, which mineralize more efficiently, and vesicles released from hFOB 1.19 cells using the TEM-EDX microanalytical method supports the hypothesis that MVs are mineral-filled vesicles. This leaves open the question whether the presence of MVs is required to induce apatite nucleation, and how this may alter physiological to pathological mineralization.

Disclosures

The authors declare that they have no conflict of interest.

Acknowledgements

MK and ASK performed manual operations and LB prepared drawings and made the movie. ASK wrote the manuscript, LB wrote the script and MK prepared the table. SM, RB and SP critically read the table, the script and the manuscript. The authors would like to thank Hanna Chomontowska for her excellent assistance with ultramicrotomy as well as Szymon Suski and Henryk Bilski for their excellent assistance with TEM-EDX analysis. The authors would like to thank dr Patrick Groves for professional English language correction and Barbara Sobiak for recording the instructions.

This work was supported by grant N N401 140639 from the Polish Ministry of Science and Higher Education to ASK, by grants from the National Science Centre, Poland 2016/23/N/NZ4/03313 to LB and 2016/23/N/NZ1/02449 to MK, EU FP7 Project BIOIMAGINE: BIO-IMAGing in research INnovation and Education, GA No. 264173, and by the statutory funds of the Nencki Institute of Experimental Biology, Polish Academy of Sciences.

References

1. Buckwalter, J.A., Cooper, R.R. Bone structure and function. *Instr. Course Lect.* **36**, 27-28 (1987).
2. Anderson, H.C. Molecular biology of matrix vesicles. *Clin. Orthop. Relat. Res.* **314**, 266-280 (1995).
3. Anderson, H.C. Matrix vesicles and calcification. *Curr. Rheumatol.* **5** (3), 222-226 (2003).

4. Bolean, M., Simão, A.M.S., Barioni, M.B., Favarin, B.Z., Sebinelli, H.G., Veschi, E.A., Janku, T.A.B., Bottini, M., Hoylaerts, M.F., Itri, R., Millán, J.L., Ciancaglini, P. Biophysical aspects of biomineralization. *Biophys Rev.* **9** (5), 747-760 (2017).
5. Bottini, M., Mebarek, S., Anderson, K.L, Strzelecka-Kiliszek, A., Bozycki, L., Simão A.M.S., Bolean M., Ciancaglini P., Bandorowicz Pikula, J., Pikula, S., Magne, D., Volkmann, N., Hanein, D., Millán, J.L., Buchet, R. Matrix vesicles from chondrocytes and osteoblasts: Their biogenesis, properties, functions and biomimetic models. *Biochim Biophys Acta.* **1862** (3), 532-546 (2018).
6. Hessle, L., Johnson, K.A., Anderson, H.C., Narisawa, S., Sali, A., Goding, J.W., Terkeltaub, R., Millan, J.L. Tissue-nonspecific alkaline phosphatase and plasma cell membrane glycoprotein-1 are central antagonistic regulators of bone mineralization. *Proc. Natl. Acad. Sci. U. S. A.* **99** (14), 9445-9449 (2002).
7. Garimella, R., Bi, X., Anderson, H.C., Camacho, N.P. Nature of phosphate substrate as a major determinant of mineral type formed in matrix vesicle-mediated *in vitro* mineralization: An FTIR imaging study. *Bone.* **38** (6), 811-817 (2006).
8. Thouverey, C., Bechkoff, G., Pikula, S., Buchet, R. Inorganic pyrophosphate as a regulator of hydroxyapatite or calcium pyrophosphate dihydrate mineral deposition by matrix vesicles. *Osteoarthr. Cartil.* **17**, 64-72 (2009).
9. Terkeltaub, R.A. Inorganic pyrophosphate generation and disposition in pathophysiology. *Am. J. Phys*. **281** (1), C1C11 (2001).
10. Guicheux, J., Palmer, G., Shukunami, C., Hiraki, Y., Bonjour, J.P, Caverzasio, J. A novel *in vitro* culture system for analysis of functional role of phosphate transport in endochondral ossification. *Bone.* **27** (1),69-74 (2000).
11. Yadav, M.C., Bottini, M., Cory, E., Bhattacharya,K., Kuss, P., Narisawa, S., Sah, R.L., Beck, L., Fadeel, B.,Farquharson, C., Millán, J.L. Skeletal mineralization deficits and impaired biogenesis and function of chondrocyte-derived matrix vesicles in Phospho1(−/−) and Phospho1/Pi t1 double-knockout mice. *J. Bone Miner. Res.* **31** (6), 1275-1286 (2016).
12. Thouverey, C., Malinowska, A., Balcerzak, M., Strzelecka-Kiliszek, A., Buchet, R., Dadlez, M., Pikula, S. Proteomic characterization of biogenesis and functions of matrix vesicles released from mineralizing human osteoblast-like cells. *J. Proteome.* **74** (7), 1123-1134 (2011).
13. Wang, W., Xu, J., Kirsch, T. Annexin-mediated Ca2+ influx regulates growth plate chondrocyte maturation and apoptosis. *J. Biol. Chem.* **278** (6),3762-3769 (2003).
14. Nollet, M., Santucci-Darmanin, S., Breuil, V., *et al.*Autophagy in osteoblasts is involved in mineralization and bone homeostasis. *Autophagy.* **10** (11), 1965-1977 (2014).
15. Boonrungsiman, S., Gentleman, E., Carzaniga, R., Evans, N.D., McComb, D.W., Porter, A.E., Stevens, M.M. The role of intracellular calcium phosphate in osteoblast-mediated bone apatite formation. *Proc. Natl. Acad. Sci. U. S. A.* **109** (35), 14170-14175 (2012).
16. Genge, B.R., Wu, L.N., Wuthier, R.E. In vitro modeling of matrix vesicle nucleation: synergistic stimulation of mineral formation by annexin A5 and phosphatidylserine. *J. Biol. Chem.* **282** (36), 26035-26045 (2007).
17. Jahnen-Dechent, W., Schäfer, B., Ketteler, M., McKee, M.D. Mineral chaperones: a role for fetuin-A and osteopontin in the inhibition and regression of pathologic calcification. *J. Mol. Med. (Berl).* **86** (4), 379-389 (2008).
18. Suchanek, W., Yoshimura, M. Processing and properties of hydroxyapatite-based biomaterials for use as hard tissue replacement implants. *J. Miner. Res.* **13** (1), 94-117 (1998).
19. Pautke, C., Schieker, M., Tischer, T., Kolk, A., Neth, P., Mutschler, W., Milz, S. Characterization of osteosarcoma cell lines MG-63, Saos-2 and U-2 OS in comparison to human osteoblasts. *Anticancer Res.* **24** (6), 3743-3748 (2004).
20. Yen, M.-L., Chien, C.-C., Chiu, I.-M., Huang, H.-I., Chen, Y.-C., Hu, H.-I., Yen, B.L. Multilineage differentiation and characterization of the human fetal osteoblastic 1.19 cell line: a possible *in vitro* model of human mesenchymal progenitors. *Stem Cells.* **25** (1), 125-131 (2007).
21. Brittle, S.W., Foose, D.P., O'Neil, K.A., Sikon, J.M., Johnson, J.K., Stahler, A.C., Ryan, J.D., Higgins, S.R., Sizemore I.E. A raman-based imaging method for characterizing the molecular adsorption and spatial distribution of silver nanoparticles to hydrated mineral surfaces. *Environ Sci Technol.* (2018).
22. Liu, N., Wang, Y., Ge, F., Liu, S., Xiao, H. Antagonistic effect of nano-ZnO and cetyltrimethyl ammonium chloride on the growth of Chlorella vulgaris: Dissolution and accumulation of nano-ZnO. *Chemosphere.* **196**, 566-574 (2018).
23. Tasbihi, M., Kočì, K., Troppová, I., Edelmannová, M., Reli, M., Čapek, L., Schomäcker, R. Photocatalytic reduction of carbon dioxide over Cu/TiO2 photocatalysts. *Environ Sci Pollut Res Int.* (2017).
24. Chen, N.X., O'Neill, K.D., Chen, X., Moe, S.M. Annexin-Mediated Matrix Vesicle Calcification in Vascular Smooth Muscle Cells. *J. Bone Miner. Res.* **23** (11), 1798-1805 (2008).
25. Strzelecka-Kiliszek, A., Bozycki, L., Mebarek, S., Buchet, R., Pikula, S. Characteristics of minerals in vesicles produced by human osteoblasts hFOB 1.19 and osteosarcoma Saos-2 cells stimulated for mineralization. *J. Inorg. Bioch.* **171,** 100-107 (2017).
26. Thouverey, C., Strzelecka-Kiliszek, A., Balcerzak, M., Buchet, R., Pikula, S. Matrix vesicles originate from apical membranę microvilli of mineralizing osteoblast-like Saos-2 cells. *J. Cell. Biochem.* **106** (1), 127-138 (2009).
27. Cazalbou, S., Eichert, D., Ranz, X., Drouet, C., Combes, C., Harmand, M.F., Rey, C. Ion exchanges in apatites for biomedical application. *J. Mater. Sci. Mater. Med.* **16** (5), 405-409 (2005).
28. Kraus, D. Consolidated data analysis and presentation using an open-source add-in for the Microsoft Excel® spreadsheet software. *Med. Writ.* **23** (1), 25-28 (2014).
29. Kawasaki, K., Buchanan, A.V., Weiss, K.M. Biomineralization in humans: making the hard choices in life. *Annu. Rev. Genet.* **43**,119-142 (2009).
30. Bonucci, E. Bone mineralization. *Front. Biosci.* **17**, 100-128 (2012).
31. Veis, A., Dorvee, J.R. Biomineralization mechanisms: A new paradigm for crystal nucleation in organic matrices. *Calcif. Tissue Int.* **93** (4), 307-315 (2013).
32. Nudelman, F., Lausch, A.J., Sommerdijk, N.A., Sone, E.D. In vitro models of collagen biomineralization. *J. Struct. Biol.* **183** (2), 258-269 (2013).
33. Alliston, T. Biological regulation of bone quality. *Curr. Osteoporos. Rep.* **12** (3), 366-375 (2014).
34. Wang, W., Kirsch, T. Retinoic acid stimulates annexin-mediated growth plate chondrocyte mineralization. *J. Cell Biol.* **157** (6), 1061-1069 (2002).
35. Wang, W., Xu, J., Kirsh, T. Annexin V and terminal differentiation of growth plate chondrocytes. *Exp. Cell Res.* **305** (1), 156-165 (2005).

